Dynamic finite-size scaling of the normalized height distribution in kinetic surface roughening

Y. Shim* and D. P. Landau
Center for Simulational Physics, University of Georgia, Athens, Georgia 30602
(Received 6 December 2000; revised manuscript received 3 April 2001; published 24 August 2001)

Using well-known simple growth models, we have studied the dynamic finite-size scaling theory for the normalized height distribution of a growing surface. We find a simple functional form that explains size-dependent behavior of the skewness and kurtosis in the transient regime, and obtain the transient- and long-time values of the skewness and kurtosis for the models. Scaled distributions of the models are obtained, and the shape of each distribution is discussed in terms of the interfacial width, skewness, and kurtosis, and compared with those for other models. Exponents η_+ and η_-, which characterize the form of the distribution, are determined from an exponential fitting of scaling functions. Our detailed results reveal that $\eta_+ + \eta_- \approx 4$ for a model obeying usual scaling in contrast to $\eta_+ + \eta_- < 4$ with $\eta_- = 1$ for a model exhibiting anomalous scaling as well as multiscaling. Since we obtain $\eta_+ + \eta_- \approx 4$ for a model exhibiting anomalous scaling but no multiscaling, we conclude that the deviation from $\eta_+ + \eta_- \approx 4$ is due to the presence of multiscaling behavior in a model.

DOI: 10.1103/PhysRevE.64.036110 PACS number(s): 05.70.Ln, 05.40.−a, 68.55.−a, 02.50.−r

I. INTRODUCTION

Kinetic roughening of growing surfaces is a well-known nonequilibrium phenomenon and has drawn much attention to the field of statistical and condensed-matter physics [1–4]. This is because of its practical applications in material fabrication and the theoretical challenge of critical behavior similar to that found in magnetic systems near the critical temperature. One of the key issues in this active area is to make a connection between experimental or simulational results and theoretical continuum growth equations derived from phenomenological arguments [1–5]. Many experiments have been performed and simple atomistic growth models that capture the key features of the system have been designed to help us understand the dynamic evolution of surface morphologies in terms of growth-related exponents that are seemingly model dependent and compared to the theoretical prediction for the system. From the theoretical perspective, the issue of understanding scaling and critical exponents for a nonequilibrium system is of great importance. The idea of self-affine scaling [6] was introduced to explain the kinetic surface roughening that evolves in a scale-invariant state with power-law behavior in characteristic length scales.

So far, a few universality classes, e.g., Edwards-Wilkinson (EW) [7], Kardar-Parisi-Zhang (KPZ) [8], molecular-beam epitaxy (MBE) class [9–11], etc., have emerged from these considerations. For example, the sedimentation of clay particles belongs to the EW universality class, whereas the Eden model [12], ballistic deposition [13], and the restricted solid-on-solid model (RSOS) [14] belong to the KPZ class. Especially, for the MBE universality class, there is an interesting point worth mentioning; with roughness and dynamic exponents characterizing surface fluctuations (interfacial width) of a growing surface, sometimes a new exponent is necessary to explain the time evolution of the mean step size unlike other models obeying usual scaling for which there is no such new exponent. This phenomenon is called anomalous scaling behavior—the local and global dynamic scaling behaviors are distinctly different [15–17]—and several experiments have reported anomalous scaling behavior in a variety of kinetic roughening systems [18–23]. Krug found a similarity between a simple 1+1-dimensional MBE model proposed by Das Sarma and Tamborenea (DT) [10] and fully developed turbulence, and showed that this DT model exhibits spatial multiscaling and its step size distribution is not a Gaussian [24]. Later simulation results, however, indicate that the DT model does not exhibit true asymptotic multiscaling [5,25].

More fundamental understanding of a dynamic process of growing films can be achieved from the normalized height-distribution function, often called the probability height-distribution function. One may be able to calculate the distribution analytically for some special cases by solving a Fokker-Planck equation obtained from a Langevin equation that governs the time evolution of height fluctuations in a growing surface [3,26–28]; however, it is very difficult to solve the Fokker-Planck equation when a nonlinear term is present in the theoretical continuum growth equations. Furthermore, obtaining the early-time behavior of the distribution is a formidable task.

Besides the analytical calculations, several experimental and simulational results for the distribution are now available. The height distribution of a film of CuCl grown on CaF_2 (111) is nearly Gaussian but slightly asymmetric once the substrate is completely covered by the incoming particle flux [29]. The terrace width distribution of a vicinal Pt surface [30] and the height distribution of a film of silver grown on a silver substrate [31] seem to be well approximated by a Gaussian function. Asymmetric behavior of the distribution is more pronounced in the simulations of a model for metal homoepitaxy with a step-edge barrier (Ehrlich-Schwoebel barrier) [32], zero-temperature-directed polymers in a random potential in several dimensions [33], and a simple

*Present address: Materials Science and Engineering Laboratory, National Institute of Standards and Technology, Gaithersburg, MD 20899; Email address: yunsic.shim@nist.gov

growth model of thin films by molecular beam epitaxy [34].

In this paper, we focus on and present results for the detailed shape of the normalized height distributions at early and late times obtained from extensive simulations of a variety of well-known simple growth models that belong to diverse universality classes. The shape of the distribution at intermediate times and in the asymptotic regime is discussed in terms of three quantities, the interfacial width, skewness, and kurtosis, all of which will be defined in the next section. We also discuss the characteristic of exponents that describe the shape of scaled distributions. In Sec. II we provide the background related to kinetic roughening and discuss models in detail that we have used. Scaling results of the distribution, skewness and kurtosis are presented and discussed in Sec. III. Section IV contains a brief summary and conclusion.

II. BACKGROUND

A. Theory

Kinetic roughening of growing surfaces is usually characterized by the interfacial width when global scaling behavior is concerned,

$$w(L,t)=\langle[h(\mathbf{r},t)-\langle h(t)\rangle]^2\rangle^{1/2}, \tag{1}$$

where $h(\mathbf{r},t)$ is the height at the lateral position $\mathbf{r}$ and time t and $\langle h(t)\rangle=(1/L^{d-1})\Sigma_{\mathbf{r}}h(\mathbf{r},t)$ for a $(d-1)$-dimensional substrate. The interfacial width has a scaling form [6]

$$w(L,t)\sim L^{\zeta}f(t/L^{z}) \tag{2}$$

with the roughness exponent ζ and the dynamic exponent z. In the asymptotic time and size regimes

$$w(L,t)\sim\begin{cases} t^{\beta} & \text{for } 1\ll t\ll L^{z} \\ L^{\zeta} & \text{for } t\gg L^{z}, \end{cases} \tag{3}$$

where $\beta=\zeta/z$. The skewness is defined as

$$S(L,t)=\langle[h(\mathbf{r},t)-\langle h(t)\rangle]^3\rangle/w(L,t)^3, \tag{4}$$

and the kurtosis is defined as

$$Q(L,t)=[\langle[h(\mathbf{r},t)-\langle h(t)\rangle]^4\rangle/w(L,t)^4]-3. \tag{5}$$

The skewness measures the asymmetry of the height distribution and the kurtosis gauges the weight contained in the tails of the distribution relative to a Gaussian [4]. Note that for a random variable with zero mean the normalized third and fourth cumulants are equal to the skewness and kurtosis, respectively [35]. Simulations of the restricted solid-on-solid model and zero-temperature-directed polymers in a random media (DPRM), which belong to the KPZ universality class, show that in the transient regime $(t/L^{z}\to 0)$, the skewness converges to $|S(0)|\approx 0.28-0.29$ [3,4,33] and for the latter DPRM model in (1+1)D, the kurtosis is $Q(0)\approx 0.12-0.16$ [4,33] unlike the standard replica calculation implying that the kurtosis $Q\equiv 0$ [36].

In addition to those quantities defined above, correlation functions can be used to determine the exponents related to the surface roughening. The height-height correlation function $G(r,t)$, which is useful when local scaling behavior is concerned, is defined as

$$G(r,t)=\langle|h(\mathbf{r}+\mathbf{r}',t)-h(\mathbf{r}',t)|^2\rangle. \tag{6}$$

When a model exhibits anomalous scaling behavior, the mean step-size function $G(r=1,t)$ has a scaling form [17]

$$G(r=1,t)\sim\begin{cases} t^{\kappa/z} & \text{for } r\ll t^{1/z}\ll L \\ L^{\kappa} & \text{for } r\ll L\ll t^{1/z}, \end{cases} \tag{7}$$

with $\kappa\neq 0$. The new exponent $\kappa=0$, however, for a model that obeys usual scaling and there is then no time t and system size L dependence in Eq. (7). It is interesting to note that when the roughness exponent $\zeta>1$, a growing surface shows super-roughening behavior (i.e., the ratio of the saturated interfacial width $w_s(L)$ to system size L, $w_s(L)/L\sim L^{\zeta-1}\to\infty$ as $L\to\infty$), and this leads to the anomalous scaling [17]; for $\zeta=1$, $G(r=1,t)\sim\ln(t)$ for $r\ll t^{1/z}\ll L$ and $\sim\ln(L)$ for $r\ll L\ll t^{1/z}$. When $\zeta<1$, however, the anomalous scaling has been also observed in the simulations of thin film growth by MBE [34,37,38]. In order to explain these unexpected results, a theoretical growth equation that has an infinite number of marginal operators has been proposed; see Refs. [4,34,39] for details.

When multiscaling behavior of a growing surface is concerned, it is useful to consider the qth order height-height correlation function $G_q(r,t)$ [24] defined as

$$G_q(r,t)=\langle|h(\mathbf{r}+\mathbf{r}',t)-h(\mathbf{r}',t)|^q\rangle^{1/q}=\xi^{\kappa_q}r^{\alpha_q}f_q(r/\xi), \tag{8}$$

where the lateral correlation length is $\xi(t)\sim t^{1/z}$ for $1\ll t\ll L^{z}$. The scaling function in Eq. (8) is $f_q(x)=\text{const}$ for $x\ll 1$ and $f_q(x)\sim x^{-\alpha_q}$ for $x\gg 1$. Note that for $q=2$, $G_2(r,t)=G(r,t)^{1/2}$ in Eq. (6) and the interfacial width $w\sim G_2(r\gg\xi)\sim\xi^{\kappa_2+\alpha_2}$. Thus, $\kappa_2=\kappa/2$ and $\kappa_2+\alpha_2=\zeta$; a general form given in Ref. [24] is $\kappa_q+\alpha_q=\zeta$. As can be seen in Eq. (8), multiscaling behavior characterized by the q-dependent roughness exponents α_q is induced by q-dependent local step-size fluctuations.

Besides the above quantities, it has been shown that the normalized height distribution of a growing surface is well approximated by the following form [32,40]

$$P_L(\Delta h(t))\sim w(L,t)^{-1}\mathcal{F}(\Delta h(t)/w(L,t)), \tag{9}$$

where $\mathcal{F}$ is a scaling function and $\Delta h(t)=h(t)-\langle h(t)\rangle$. Note that for a Gaussian height distribution $P(\Delta h(t))=[\sqrt{2\pi}w(t)]^{-1}\exp[-\Delta h^2(t)/2w^2(t)]$, $S(t)=0$ and $Q(t)=0$. Using Eq. (3) we find that the normalized height distribution function in Eq. (9) can be further simplified in two limiting cases, i.e., at intermediate times and in the asymptotic regime as

$$P_L(\Delta h(t))\sim\begin{cases} t^{-\beta}\mathcal{F}_1(\Delta h(t)/t^{\beta}) & \text{for } 1\ll t\ll L^{z} \\ L^{-\zeta}\mathcal{F}_2(\Delta h(t)/L^{\zeta}) & \text{for } t\gg L^{z}, \end{cases} \tag{10}$$

where $\mathcal{F}_1(x_1)$ and $\mathcal{F}_2(x_2)$ are scaling functions with the arguments x_1 and x_2, respectively. Thus the detailed shape of the scaling functions in both regimes can be obtained from data collapse, i.e.

$$\mathcal{F}_1(x_1) \sim t^{\beta} P_L(\Delta h(t)) \quad \text{for } 1 \ll t \ll L^z \tag{11}$$

$$\mathcal{F}_2(x_2) \sim L^{\zeta} P_L(\Delta h(\infty)) \quad \text{for } t \gg L^z, \tag{12}$$

where $x_1 = \Delta h(t)/t^{\beta}$ and $x_2 = \Delta h(\infty)/L^{\zeta}$ with $\Delta h(\infty) = \Delta h(t \gg L^z)$.

The scaling functions $\mathcal{F}_1(x_1)$ and $\mathcal{F}_2(x_2)$ seem to be well approximated by an exponential function with the arguments x_1 and x_2 [3]. At intermediate times,

$$\mathcal{F}_1(x_1) \sim \begin{cases} \exp[-a_+ x_1^{\eta_+}] & \text{for } x_1 > 0 \\ \exp[-a_- x_1^{\eta_-}] & \text{for } x_1 < 0 \end{cases} \tag{13}$$

and for the long-time asymptotic (finite-size rounded) regime,

$$\mathcal{F}_2(x_2) \sim \begin{cases} \exp[-b_+ x_2^{\eta_+}] & \text{for } x_2 > 0 \\ \exp[-b_- x_2^{\eta_-}] & \text{for } x_2 < 0, \end{cases} \tag{14}$$

where $a_{\pm}$ and $b_{\pm}$ are constant in each case. If $\eta_+ = \eta_- = 2$, then the distribution is simply Gaussian and reflects the central limit theorem in statistics. Halpin-Healy and Zhang [3,41] obtained the distribution functions of interfaces in a random media, using a replica scaling analysis. His result shows that in (1+1)D, the exponents $\eta_+ = 5/2$ and $\eta_- = 3/2$ for $1 \ll t \ll L^z$, and $\eta_+ = \eta_- = 2$ for $t \gg L^z$ with $\zeta = 1/2$ and $z = 3/2$. It is interesting to note that in the asymptotic regime, the height distribution of the interfaces in a random media is Gaussian and $\eta_+ + \eta_- = 4$ in both regimes.

B. Models

We have simulated a variety of simple growth models to determine the scaling form and shape of the normalized height distribution. Figure 1 shows a schematic rule for diffusion for a freshly deposited particle in each model in (1+1)D, and it is straightforward to extend the growth algorithms to higher dimensions. In our simulations, we have used periodic boundary conditions and a growth process starts with a flat $(d-1)$-dimensional substrate at time $t=0$, i.e., $h(\mathbf{r}, t=0) = 0$, in all the models.

1. Restricted solid-on-solid (RSOS) model

The growth of a surface proceeds by increasing the height $h(\mathbf{r})$ by one, i.e., $h(\mathbf{r}) \rightarrow h(\mathbf{r}) + 1$ on a randomly selected site $\mathbf{r}$ provided that the neighboring height difference $|\Delta h| = 0,1$ is obeyed at all stages. This rather simple growth model produces a compact surface with excellent scaling. Simulations yielded $\zeta(d) = 2/(d+2)$ and $z(d) = 2(d+1)/(d+2)$ [14]. It is also known that the (1+1)D RSOS model is well described by the KPZ equation

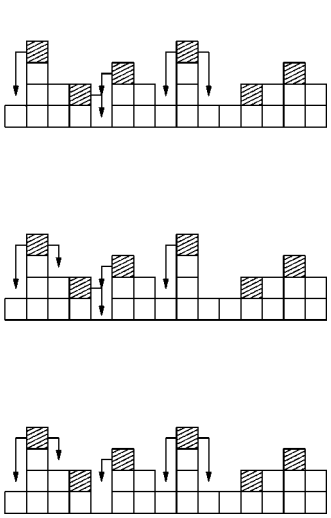

FIG. 1. A schematic rule for diffusion for three growth models in (1+1)D. The arrows show possible different paths. (a) The Edwards-Willkinson (EW) model, (b) the Wolf-Villain (WV) model, and (c) the Das Sarma-Tamborenea (DT) model.

$$\frac{\partial h}{\partial t} = \nu \nabla^2 h + \frac{\lambda}{2} (\nabla h)^2 + \eta(\mathbf{r}, t), \tag{15}$$

where $\eta(\mathbf{r}, t)$ is assumed to be a δ-correlated Gaussian white noise. However, in 2+1D the exact solution of the KPZ equation has not been obtained and only approximate solutions by renormalization group and self-consistent calculations are available.

2. Edwards-Wilkinson (EW) model

A freshly landed particle on a randomly selected site denoted by a square with slanted lines shown in Fig. 1(a) seeks the lowest height in the nearest-neighbor sites and diffuses to the site provided that it has lower height than the presently occupied site. If there are two equally probable sites providing the same lower height, then the particle chooses one of them randomly and relaxes to the site. If there is no such site, then the particle stays there and becomes immobile. Edwards and Wilkinson discussed their model in detail in their pioneering work [7], but the atomistic simulation of the EW model was first done by Family [42]. The EW model is well described by the EW equation

$$\frac{\partial h}{\partial t} = \nu \nabla^2 h + \eta(\mathbf{r}, t), \tag{16}$$

which yields $\zeta(d) = (3-d)/2$ and $z = 2$ [7,43]. Note that in 2+1D, the nature of the diffusion in the atomistic model is important in determining its relationship to the EW equation [44].

3. Wolf-Villain (WV) model

A freshly deposited particle on a randomly selected site seeks a nearest-neighbor site providing a maximum coordination number and moves to that site as shown in Fig. 1(b). If there are two equally probable sites [in (1+1)D], then the

particle chooses one of them randomly. If there is no such site, then the particle stays there and becomes immobile. Since in the WV model [9], each particle looks to increase its bonds with neighbor sites, at long times and for large system size, a site at a valley on a surface tends to be more preferable for a particle to diffuse to than the one on the top of hill. This movement induces a downhill current and the WV model exhibits a crossover to the EW behavior, however, the crossover only appears at long times and for large systems [45]. Note that unlike the previously introduced RSOS and EW models that exhibit usual scaling, this WV model exhibits anomalous scaling with $\kappa/z=0.38$ [16] at early times ($\ll$ the crossover time t_c), but which is transient behavior before the crossover.

4. Das Sarma-Tamborenea (DT) model

A freshly deposited particle having only one nearest-neighbor bond seeks a neighboring site providing more bonds than the present one and diffuses to that site as shown in Fig. 1(c). If the present site has more than one bond, then the particle becomes immobile. If there are two neighboring sites [in (1+1)D] providing more bonds regardless of the number of bonds, then the particle chooses one of them randomly and moves to the site. The continuum growth equation for the DT model [10] turns out be more complicated than initially thought. It is worth noting that the WV and DT models have been initially suggested to describe the growth of thin films by MBE with the fourth-order linear Langevin equation (often called Mullins-Herring (MH) equation [46])

$$\frac{\partial h}{\partial t}=-\kappa_0\nabla^4 h+\eta(\mathbf{r},t). \tag{17}$$

Later, however, anomalous scaling behavior has been reported in the WV and DT models with different growth equations from Eq. (17) [15,16]. Especially, the DT model in (2+1)D exhibits a crossover at late times and yields the same values of ζ and z [5] as those ($\zeta=2/3$ and $z=10/3$) obtained from the Lai–Das Sarma–Villain (LDV) growth equation [11,47]

$$\frac{\partial h}{\partial t}=-\kappa_0\nabla^4 h+\lambda_1\nabla^2(\nabla h)^2+\eta(\mathbf{r},t). \tag{18}$$

It has been shown that the ratio of the anomalous exponent κ to the dynamic exponent z, $\kappa/z\approx 0.4$ for the (1+1)D DT model [17]. The same model in 2+1D shows that the ratio, $\kappa/z\to 0$ long before the interfacial width saturates; however, the long-lived transient behavior is much stronger in (1+1)D [5]. This result indicates that the anomalous scaling may be transient behavior, and asymptotically $\kappa\to 0$. Also note that the LDV equation yields $\zeta=1$ in (1+1)D, and thus, results in logarithmic anomalous scaling.

In our simulation of the DT model, we focus our attention on a rather small system that exhibits anomalous scaling as well as multiscaling since the detailed discussion of the crossover is beyond our scope of this paper (and crossover is very difficult to detect).

5. Absolute solid-on-solid (ASOS) model

In this model [48], key parameters are the temperature T and deposition probability τ with the Hamiltonian $\mathcal{H}=(J/2)\Sigma_{\langle \mathbf{r},\mathbf{r}'\rangle}|h(\mathbf{r})-h(\mathbf{r}')|$, where $\langle \mathbf{r},\mathbf{r}'\rangle$ denotes the nearest-neighbor summation in a $(d-1)$ dimensional substrate. First, a random number rnd is generated, and if the number $rnd\leqslant\tau$, then a particle is deposited on a randomly selected site $\mathbf{r}$; otherwise, the particle on that site attempts surface diffusion. The diffusion movement is accepted with the transition probability $W(\mathbf{r}\to\mathbf{r}')$ to a randomly selected nearest-neighbor site $\mathbf{r}'$

$$W(\mathbf{r}\to\mathbf{r}')=[1+\exp(-\Delta\mathcal{H}/k_{\mathrm{B}}T)]^{-1},$$

where $\Delta\mathcal{H}$ is the energy difference between before and after diffusion. We specifically choose this model as an example in order to compare its scaled distribution with that of the above EW model since this ASOS model belongs to the EW universality class [48]. In our simulation, we used the temperature $T=1J/k_{\mathrm{B}}$ and deposition probability $\tau=0.1$ in (1+1)D that are the same as in Ref. [48].

6. Molecular-beam epitaxy (MBE) growth model

In this model [48], the diffusion process is thermally activated and reversible. There are two important time scales in this film growth simulation; one is for particle deposition and the other is for surface diffusion. δt is time between the successive deposition of particles and τ_{D} is time between the successive surface diffusion events during the time interval δt. Therefore, the total number of events T_{e} occurring during the time interval δt is proportional to the sum of the total number of particle deposition (F) and diffusion (D) during deposition of one monolayer (ML). If one chooses the unit of particle-beam flux (F) as 1 ML/sec, then during 1 sec, the total number of events is

$$T_{\mathrm{e}}=F+D,$$

where the diffusion constant D is measured in the unit of per site per second (1/site/s). Here, probability for particle deposition is $\tau=F/T_{\mathrm{e}}=1/(1+D/F)$ and probability for surface diffusion is $1-\tau$. Thus, the ratio D/F is one of the key parameters determining surface morphologies.

The simulation process of this model is rather simple. First, a site is selected randomly, and then a particle is deposited on the selected site with probability τ; otherwise, the particle at that site tries to diffuse to one of the nearest-neighbor sites. The transition probability $W(\mathbf{r}\to\mathbf{r}')$ is given as

$$W(\mathbf{r}\to\mathbf{r}')=\exp[-E_n(\mathbf{r})/k_{\mathrm{B}}T],$$

where the effective binding energy, $E_n(\mathbf{r})=nJ$ with $J>0$ and n is the number of lateral bonds with $n=0,1,2,3,4$ in a two-dimensional substrate (simulations have been done in 2+1 dimensions). Once an atom overcomes the energy barrier $E_n(\mathbf{r})$, it diffuses to one of the nearest-neighbor sites randomly with probability 1/4. It has been shown that the

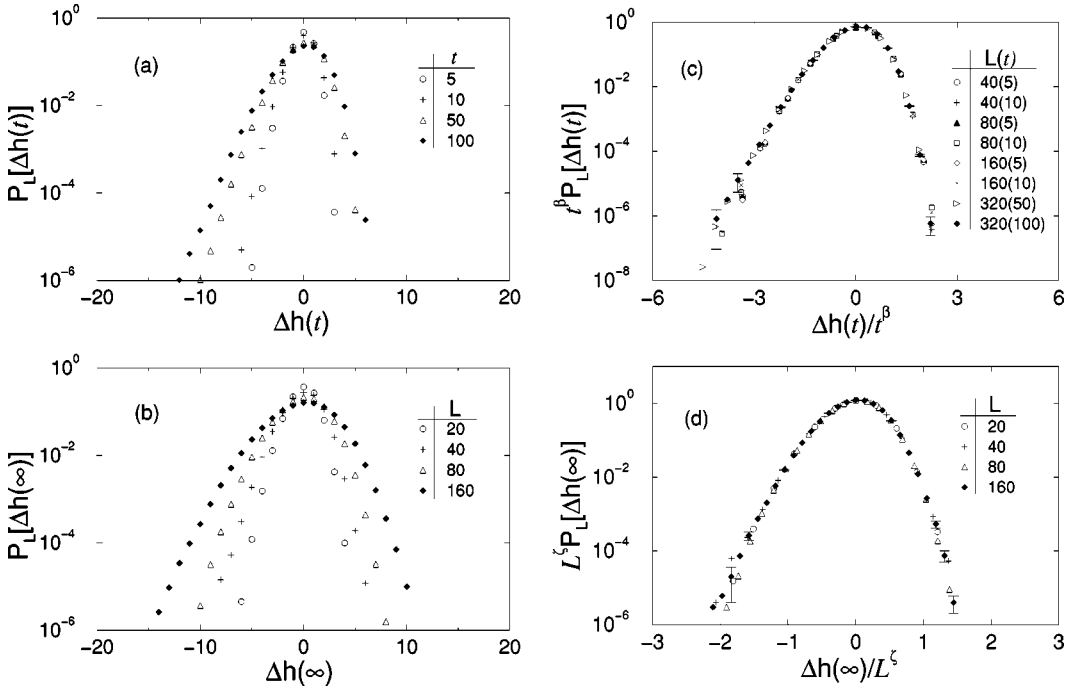

FIG. 2. Time- and size-dependent behavior of the normalized height distributions and their scaling plots for the (2+1)D RSOS model. (a) Time- and (b) size-dependent behavior of the distribution. Scaling plots (c) at intermediate times with $\beta=1/4$ and (d) in the asymptotic regime with $\zeta=0.4$.

Arrhenius type of surface diffusion breaks the up-down symmetry [48], possibly resulting in nonzero skewness.

All the length scales have been measured in the unit of lattice constant a and time t is measured in units of monolayers (ML) deposited. Simulations have been performed on Linux workstations with the random number generator, *ran2*, given in Ref. [49]. Many averages have been taken to reduce statistical errors below 5%, especially in a calculation of the normalized height distribution that requires more averages; for example, 21 000 (3000) different runs have been averaged for $L=100$ (160) with a different random number seed for the (1+1)D DT model.

III. RESULTS

As mentioned in the introduction, our focus is on detailed scaling behavior of the normalized height distribution of each model and the difference between models obeying usual and anomalous scaling. We first start with models obeying usual scaling.

A. Usual scaling

Figure 2 shows time- and size-dependent behavior of the normalized height distributions and their scaling plots for the (2+1)D RSOS model at intermediate times [$w(t)\sim t^{\beta}$ with $\beta=1/4$] and in the asymptotic regime [$w_s(L)\sim L^{\zeta}$ with $\zeta=0.4$]. Those values of the exponents β and ζ that we obtained are the same as those reported in Ref. [14]. The maximum of the distribution decreases due to the increase in surface fluctuations as growth proceeds, and reaches a steady-state value due to the saturation of surface fluctuations in a finite size of system, as shown in Figs. 2(a) and 2(b). Note that the maxima of the distributions are at $\Delta h(t)=0$, i.e., $h(t)=\langle h(t)\rangle$. We have also obtained excellent scaling for the interfacial width $w(L,t)$ and for $P_L(t)\equiv P_L(\Delta h(t)=0)$ with $\zeta=0.4$ and $z=1.6$. The scaling of $P_L(t)$, i.e., $L^{\zeta}P_L(t)$ *vs* t/L^z, clearly demonstrates that $P_L(t)\sim w(L,t)^{-1}$, a feature that we do not show here to avoid overcrowding of figures. This relationship can be also obtained from Eq. (9) in which the scaling function $\mathcal{F}(\Delta h(t)/w(L,t))$ is constant when $\Delta h(t)=0$. This result implies that the time-dependent normalized height distribution can be also used to extract the exponents characterizing the universality class of the system.

The scaled distributions at intermediate times and in the asymptotic regime shown in Figs. 2(c) and 2(d) are asymmetric, but the former case is slightly more skewed, indicating that the magnitude of the skewness at intermediate times is larger than that for the latter case. Figure 3 shows the scaling results for the skewness S and kurtosis Q for the RSOS and EW models. For the (2+1)D RSOS model, we obtained $S=-0.23\pm0.02$ and $Q=-0.15\pm0.02$ in the asymptotic regime, shown in Figs. 3(a) and 3(b). On the other hand, for the (1+1)D RSOS model, the asymptotic value of the skewness is $S\approx0$ with $z=1.5$, which is the same as that presented in Ref. [3]. The asymptotic scaled kurtosis for the (1+1)D RSOS model, shown in Fig. 3(c), is $Q=-0.61\pm0.02$.

Unlike the (2+1)D RSOS model, the maximum of the scaled height distribution of the 1+1D RSOS model at intermediate times does not appear to be at $\Delta h(t)=0$, although we cannot exclude this possibility considering the error bars. A similar result has been also observed in Ref. [33]. How-

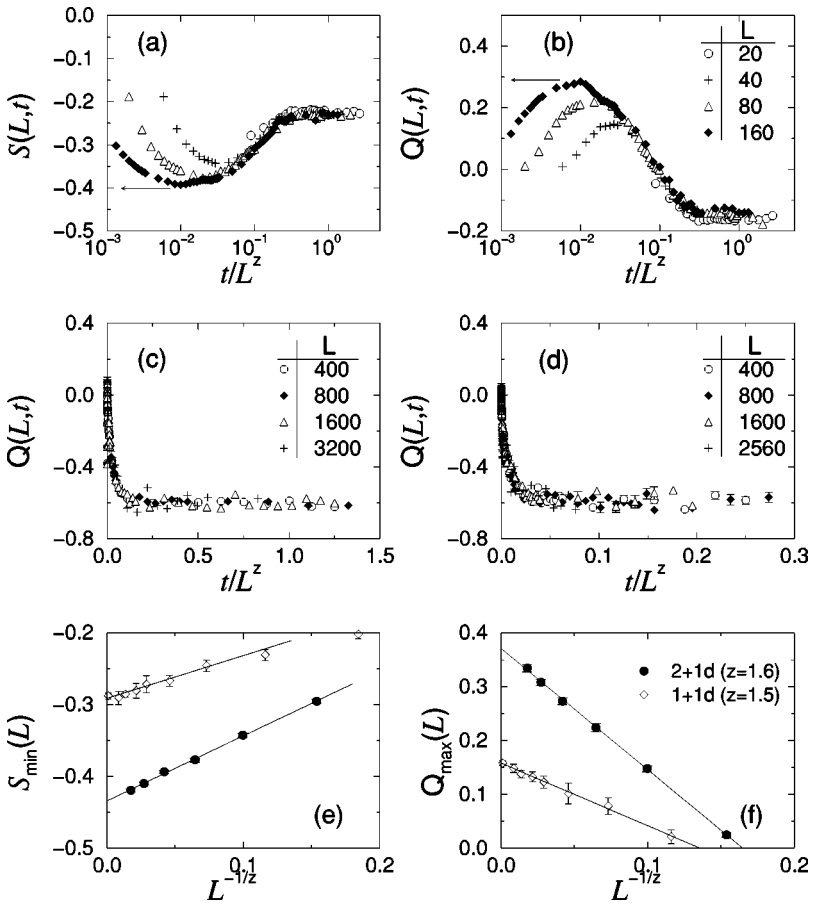

FIG. 3. Scaling plots of the skewness and kurtosis for the RSOS and EW models. (a) The skewness $S=-0.23\pm0.02$ and (b) the kurtosis $Q=-0.15\pm0.02$ in the asymptotic regime for the (2+1)D RSOS model with $z=1.6$. Arrows in (a) and (b) show the minimum and maximum values of the skewness and kurtosis for $L=160$, respectively. (c) The asymptotic kurtosis $Q=-0.61\pm0.02$ for the (1+1)D RSOS model with $z=1.5$ and (d) $Q=-0.60\pm0.03$ for the (1+1)D EW model with $z=2$. The transient-time ($t/L^z\rightarrow0$) (e) skewness and (f) kurtosis for the (1+1)D and (2+1)D RSOS model. In the thermodynamic limit, $S(0)=-0.434\pm0.002$ and $Q(0)=0.370\pm0.002$ in (2+1)D with $20\leqslant L\leqslant640$ and $S(0)=-0.292\pm0.002$ and $Q(0)=0.157\pm0.002$ in (1+1)D with $200\leqslant L\leqslant10^6$; in the (1+1)D case, 10 has been multiplied to $L^{-1/z}$ for clarity.

ever, this behavior does not exist in the (1+1)D EW model in which the scaled skewness yields both $S(t\ll L^z)$ and $S\approx0$ with $\zeta=1/2$ and $z=2$, but as shown in Fig. 3(d), the kurtosis $Q=-0.60\pm0.03$ in the asymptotic regime. Note that those asymptotic values for the (1+1)D EW model are almost the same as those for the (1+1)D RSOS model. For the (1+1)D ASOS model, we find $S\approx0$ and $Q\sim-0.58$ in the asymptotic regime for the largest system size ($L=320$) that we have simulated. This result for the ASOS model, that the asymptotic values of the skewness and kurtosis with $\zeta=1/2$ and $z=2$ are almost the same as those for the (1+1)D EW model, is not surprising since the model belongs to the EW universality class.

The transient-time ($t/L^z\rightarrow0$) behavior of the skewness and Kurtosis for the RSOS model in (2+1)D [as well as in (1+1)D] are shown in Figs. 3(e) and 3(f), where we plotted the minimum value of the skewness $S_{\min}(L,t)$ and the maximum value of the kurtosis $Q_{\max}(L,t)$— denoted by arrows in (a) and (b) as an example for $L=160$—as a function of $L^{-1/z}$. As can be seen in Figs. 3(e) and 3(f), there is simple size-dependent behavior in the transient-time skewness and kurtosis such that

$$S(0)-S_{\min}(L,t)\sim L^{-1/z} \quad \text{and} \quad Q(0)-Q_{\max}(L,t)\sim L^{-1/z}, \tag{19}$$

where $S(0)$ and $Q(0)$ are the transient-time skewness and kurtosis in the thermodynamic limit, respectively. Note that Eq. (19) explains the data well and yields $S(0)=-0.434\pm0.002$ and $Q(0)=0.370\pm0.002$ in (2+1)D and $S(0)=-0.292\pm0.002$ and $Q(0)=0.157\pm0.002$ in (1+1)D for RSOS model; the latter results are consistent with those in Ref. [33]. It is worth noting that Eq. (19) implies that the dynamic exponent z can be obtained from the early-time result of the skewness or kurtosis.

The height distributions of the (2+1)D EW model at intermediate times and in the asymptotic regime are also Gaussian as expected. It is interesting to note that at early times, the skewness and kurtosis oscillate around zero with a period of 1 ML due to the quasi layer-by-layer growing nature of the model, and then decay to zero at late times. The relative phase difference between the oscillating skewness and kurtosis is 1/4 ML simply because the skewness is an odd function but the kurtosis is an even function.

In order to obtain the detailed form of the scaled distributions in Fig. 2, we have fitted them to the exponential functions given in Eqs. (13) and (14). Figure 4 shows the exponents η_+ and η_- for the (2+1)D RSOS model at intermediate times (a) and in the asymptotic regime (b). Power-law fits to the data yield $\eta_+=2.6\pm0.2$ and $\eta_-=1.5\pm0.1$ in (a) and $\eta_+=2.3\pm0.2$ and $\eta_-=1.67\pm0.13$ in (b). The results of fits for the RSOS, EW, and ASOS models as well as the transient- and long-time values of the skewness S are given in Table I.

As can be seen in Table I, in the asymptotic regime, the values of the exponents η_+ and η_- for the (1+1)D RSOS model are the same as those for the (1+1)D EW model

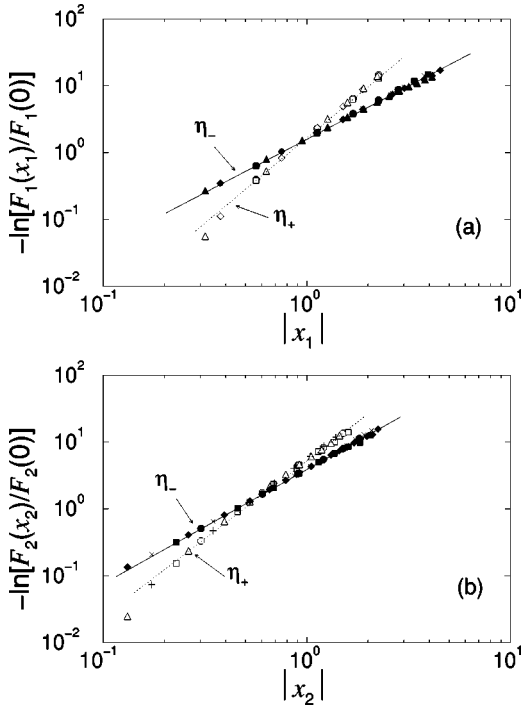

FIG. 4. The exponents η_+ and η_- obtained from an exponential fit with $\beta=1/4$ and $\zeta=0.4$ for the (2+1)D RSOS model. The solid (dotted) line is a power-law fit, yielding the exponents η_+ (η_-). (a) $\eta_+=2.6\pm0.2$ and $\eta_-=1.5\pm0.1$ at intermediate times with $x_1=\Delta h(t)/t^{\beta}$ and (b) $\eta_+=2.3\pm0.2$ and $\eta_-=1.67\pm0.13$ in the asymptotic regime with $x_2=\Delta h(\infty)/L^{\zeta}$.

within the error bars with the same values of the roughness exponent, skewness, and kurtosis. Our simulation result for the (1+1)D RSOS and EW models in the regime, that both distributions are well approximated by Gaussian, is consistent with the (1+1)D steady-state theoretical solutions of Fokker-Planck equations for the KPZ and EW equations—both yield a Gaussian height distribution [3]. However, we find a discrepancy in the asymptotic kurtosis between the theoretical solutions (implying $Q=0$) and simulation results for the models ($Q\approx-0.6$). It should be noted that nothing is known about the preasymptotic regime even in the (1+1)D KPZ problem except that the up-down symmetry must be broken due to an explicit nonlinear symmetry breaking term in the KPZ equation.

It is clear from Table I that when the skewness is zero, the distribution is well described by a Gaussian function (except its tails) with $\eta_+=\eta_-\approx2$. If we examine the value of the exponents η_+ and η_- as a function of the skewness S, we can easily confirm that a deviation from the Gaussian distribution is determined by the strength of nonzero skewness. Another interesting point is that the sum of the exponents η_+ and η_- is $\eta_++\eta_-=4$ within the error bars, a feature that may be an artifact of the central limit theorem in statistical physics that yields a Gaussian distribution. Note that the central limit theorem is valid if random variables are all similar and there is no dominant (or only a small number of dominant) one than others [50].

B. Anomalous scaling

We first show the time evolution of the normalized height distribution of the (1+1)D DT model in Fig. 5(a). The maximum of the distribution decreases due to the increase in surface fluctuations (the interfacial width) as time t increases, and reaches its steady-state value as the interfacial width saturates. Note that the locations of the maxima of the distributions are not at $\Delta h(t)=0$ but shift to the right, depending on time t. Figure 5(b) shows the shift $\delta h(L,t)$, which is defined as the location of the maximum measured from zero in the x axis, as a function of system size L and time t. For small time $t<10^2$ the shift is about one lattice constant and then increases before saturating at late times. At intermediate times, the shift $\delta h(t)\sim t^{\phi}$ with $\phi=0.38\pm0.02$, and in its steady state $\delta h(L)\sim L^{\alpha}$ with $\alpha=1.48\pm0.07$, shown in the inset of Fig. 5(b). The values of ϕ and α that we have obtained for the shift $\delta h(L,t)$ are almost the same as $\beta=0.375$ and $\zeta\approx1.47$, respectively, obtained from the interfacial width $w(L,t)$ given in Ref. [10]. This result simply implies that $\delta h(L,t)\sim w(L,t)$.

Similar behavior in the shift $\delta h(L,t)$ with $\phi\sim0.38$ has been observed in the (1+1)D WV model. Due to the crossover to the EW behavior after $t_c\approx10^6$ [45], we have plotted the ratio of $\delta h(L)$ to $w_s(L)$ instead of plotting $\delta h(L,t)$ itself in the asymptotic regime. As shown in Fig. 6, the ratio $\delta h(L)/w_s(L)$ is constant for $40\leqslant L\leqslant120$ within the error bars, and decreases slightly for $L\geqslant120$. The trend of the decrease in the ratio for a rather large system size L is easily explained because it is expected that for $t>t_c$, $\delta h(L)/w_s(L)\to0$ due to the crossover; $\delta h(L)\to$constant but $w_s(L)\sim L^{1/2}\to\infty$ as $L\to\infty$. We also calculated the qth-order height-height correlation function $G_q(r,t)$ for the (1+1)D WV model to check multiscaling behavior. Our result for L

TABLE I. The values of the exponents η_+ and η_- and the skewness $S(L,t)$ for various growth models at intermediate times ($1\ll t\ll L^z$) and in the asymptotic regime ($t\gg L^z$). The exponents η_+ and η_- for the (2+1)D EW model are determined by a Gaussian fit to the data.

		$1\ll t\ll L^z$			$t\gg L^z$		
Model	Dimension	$S(0)$	η_+	η_-	S	η_+	η_-
EW	1+1	$\simeq0$	2.0 ± 0.1	2.0 ± 0.1	$\simeq0$	2.0 ± 0.1	2.0 ± 0.1
EW	2+1	$\simeq0$	2	2	$\simeq0$	2	2
ASOS	1+1	$\simeq0$	$\simeq2$	$\simeq2$	$\simeq0$	$\simeq2$	$\simeq2$
RSOS	1+1	-0.292 ± 0.002	2.4 ± 0.2	1.7 ± 0.2	$\simeq0$	2.1 ± 0.2	2.0 ± 0.2
RSOS	2+1	-0.434 ± 0.002	2.6 ± 0.2	1.5 ± 0.1	-0.23 ± 0.02	2.3 ± 0.2	1.67 ± 0.13

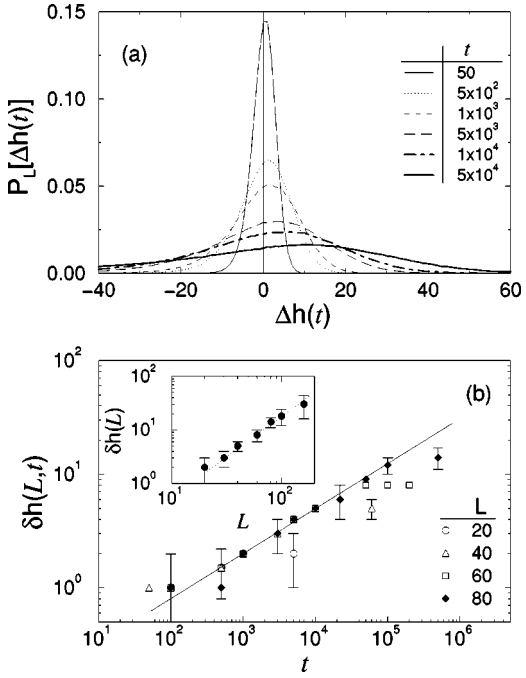

FIG. 5. The time evolution of the normalized height distribution and the shift $\delta h(L,t)$ in the distributions for the (1+1)D DT model. (a) The normalized height distribution $P_L[\Delta h(t)]$ for system size $L=80$ as a function of six different time t. (b) The shift $\delta h(L,t)$ in the time-dependent distributions shown in (a) as a function of system size L and time t. The solid line is a power-law fit to the data with $\delta h(t) \sim t^{0.38\pm0.02}$. The inset in (b) shows the shift $\delta h(L)$ in the asymptotic regime. The dotted line in the inset is a power-law fit with $\delta h(L) \sim L^{1.48\pm0.07}$.

$=10^4$ at $t=10^4 (\ll t_c)$ shows that the model exhibits multiscaling [51], but that is transient behavior before the crossover to the EW behavior.

The scaled height distributions of the (1+1)D DT model at intermediate times and in the asymptotic regime are presented in Fig. 7. In order to make the maxima of the scaled distributions be at zero on the x axis, constants a_1 and a_2 have been subtracted. With $\zeta=1.45$ and $\beta=0.375$ excellent

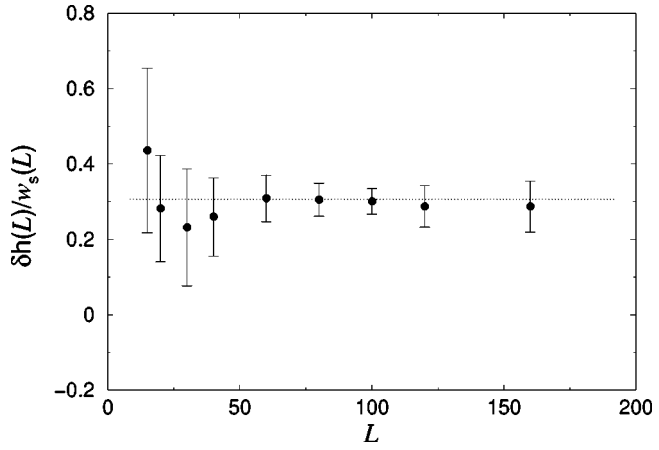

FIG. 6. The ratio of the steady-state shift $\delta h(L)$ to the saturated interfacial width $w_s(L)$ for the (1+1)D WV model.

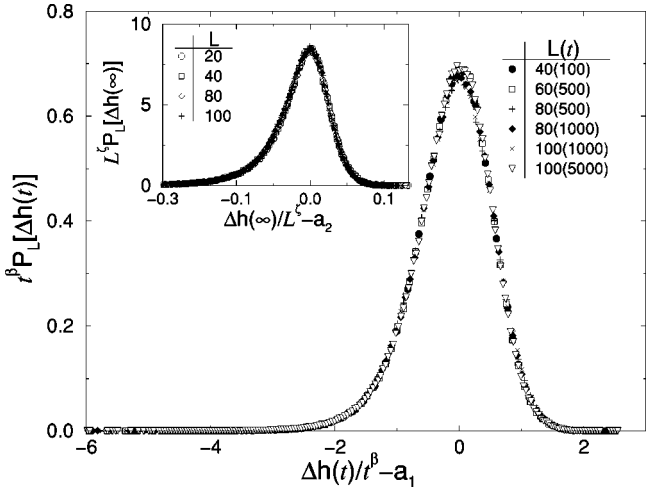

FIG. 7. Scaling plots of the normalized height distribution at intermediate times and in the asymptotic regime shown in the inset for the (1+1)D DT model. Here, $\beta=0.375$ and $\zeta=1.45$ with the constants $a_1=0.12$ and $a_2=0.022$.

scaling has been obtained in both regimes. The scaled distributions in both regimes appear to be asymmetric, indicating that the skewness is nonzero; indeed, $S(t)=-0.50\pm0.01$ for $10^2 \leqslant t \leqslant 10^6$ and $L=320$. We have obtained excellent scaling for the interfacial width $w(L,t)$ and for $P_L(t)$ with $\zeta=1.47$ and $z=4$ for system size $L \leqslant 80$. We have also observed a very slow crossover from $\beta=0.375$ to $\beta=0.333$ at late times with a change in $\zeta \approx 1.5$ to a lower value (probably $\zeta=1$) in (1+1)D as L becomes larger. However, the crossover is not so manifest, but rather quite slow in the range of system sizes and time t that we have simulated.

The exponents η_+ and η_- for the scaled distribution of the (1+1)D DT model, shown in Fig. 7, are given in Fig. 8 where $x_1=\Delta h(t)/t^{\beta}-a_1$ and $x_2=\Delta h(\infty)/L^{\zeta}-a_2$. It turns out that at intermediate times, $\eta_+=2.03\pm0.12$, and in the asymptotic regime, $\eta_+=1.90\pm0.16$ when both x_1 and $x_2>0$, indicating that the distributions for those x_1 and x_2 seems to be well approximated by a Gaussian function. When both x_1 and $x_2<0$, however, the Gaussian behavior with $\eta_- \approx 2$ is manifest only near the maxima, but as $|x_1|$ and $|x_2|$ (where both x_1 and $x_2<0$) become larger, the distributions are no longer Gaussian; η_- deviates from 2 in both cases. It is quite clear from the insets of Figs. 8(a) and 8(b) that the exponent $\eta_-=1$ when x_1 and $x_2<0$ (but not near the maxima), i.e., the distributions are pure exponential functions. Based on these results, the relation $\eta_+ + \eta_- \approx 4$ is not valid, but rather $\eta_+ + \eta_- \approx 3$ in both regimes. For the (1+1)D WV model, we observed very similar behavior in the height distributions and obtained $\eta_+=1.85\pm0.1$ and $\eta_-=1$ for $L \leqslant 160$ in the asymptotic regime. Note that the DT and WV models exhibit multiscaling in the range of system size and time that we used in the calculation.

Figure 9 shows the normalized height distributions of the (2+1)D MBE growth model in the asymptotic regime for the temperatures $k_BT/J=0.234$ and 1. The distribution at the temperature $k_BT/J=0.234$ is not Gaussian but rather an asymmetric skewed function (the skewness, $S \simeq -0.61$ for

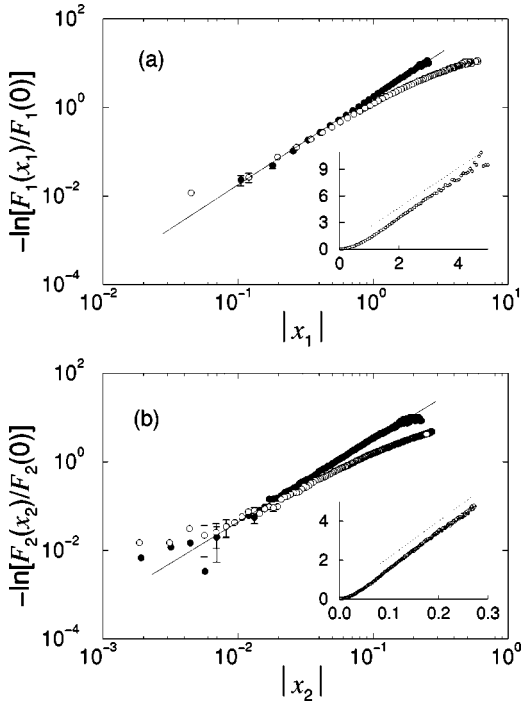

FIG. 8. The exponents η_+ and η_- obtained from an exponential fit for the scaling results shown in Fig. 7. (a) At intermediate times $[x_1=\Delta h(t)/t^{\beta}-a_1]$ with $L=100$ and $t=10^3$. Filled (open) circles are for $x_1>0$ ($x_1<0$). The solid line is a power-law fit to the data for $x_1>0$, yielding $\eta_+=2.03\pm0.12$. The inset is a linear plot of the data for $x_1<0$, and the dotted line is a guide line to the data. (b) In the asymptotic regime $[x_2=\Delta h(\infty)/L^{\zeta}-a_2]$ with $L=100$. Filled (open) circles are for $x_1>0$ ($x_1<0$). The solid line is a power-law fit to the data for $x_1>0$, yielding $\eta_+=1.90\pm0.16$. The inset is a linear plot for the data for $x_1<0$, and the dotted line is a guide line to the data.

$L=60$). The location of the maximum of the distribution for $k_BT/J=0.234$ does not seem to be at $\Delta h(\infty)=0$ but rather at $\Delta h(\infty)=2$ even though it may be indistinguishable within the error bars. The scaling analysis of the distribution shows almost the same result that shown in Fig. 8(b) with $\eta_+=2.17\pm0.20$ and $\eta_-=1$ where $\eta_++\eta_-\approx3.2$; see the inset of Fig. 9.

For $k_BT/J=0.234$, we have observed anomalous scaling [52] as well as multiscaling behavior (see Fig. 10) with $\zeta=0.7$ and $z=3.4$. Note that these values of the exponents, ζ and z, are close to the theoretical prediction of the LDV equation. As can be seen in the inset of Fig. 10 for $G_q(r=1,t)$, the curvature of the dotted lines indicates that the multiscaling as well as anomalous scaling behavior observed at this temperature seem to be transient due to a long crossover (probably to $\kappa_q\approx0$ in the long-time asymptotic regime): indeed, $G_q(r=1,t)\sim\ln(t)$ for $10^3\leqslant t\leqslant10^4$ due to $\kappa_q/z\approx0$, but this may not be the true asymptotic behavior. Note that a power-law fit to the data for the region does not yield $\kappa_q+\alpha_q\approx\zeta$, but we have observed a systematic deviation from that. The curvature does not result from finite-size saturation since $w(t)\sim t^{\beta}$ with $\beta\approx1/5$ for $L=80$ and $30\leqslant t\leqslant10^4$, and thus implies that in the limit of $t\to\infty$, $G_q(r=1,t)\sim$const because $\zeta<1$. It is interesting to note that in a

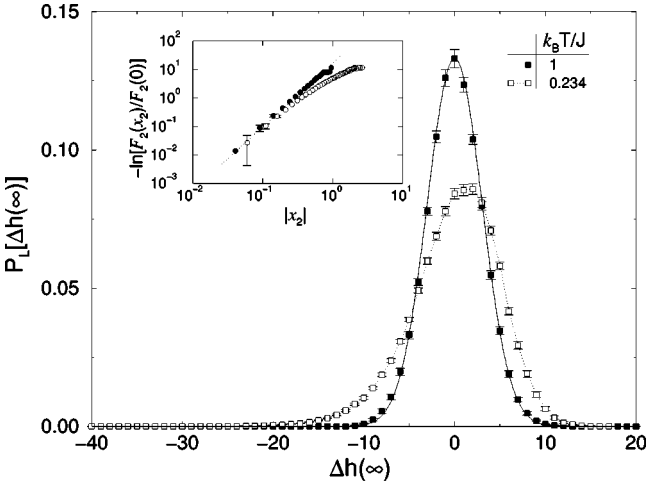

FIG. 9. The normalized height distribution of the (2+1)D MBE growth model in the asymptotic regime. Here, the temperature $k_BT/J=0.234$ and 1, $L=60$, and $D/F=10^2$. The solid line is a Gaussian fit to the data for $k_BT/J=1$ with $P(x)=0.133\exp[-0.0548x^2]$ which explains the data well and implies $\eta_+=\eta_-=2$. The inset shows the exponents η_+ and η_- for the temperature $k_BT/J=0.234$, where $x_2=\Delta h(\infty)/L^{\zeta}-a_2>0$ with $\zeta=0.7$ and $a_2=0.13$. Filled (open) circles are for $x_2>0$ ($x_2<0$). The dotted line in the inset is a power-law fit to the data for $x_2>0$, yielding $\eta_+=2.17\pm0.20$. A linear plot of the inset yields $\eta_-=1$, which is not shown here to avoid overcrowding of figures.

range of system size and time ($L\leqslant80$ and $t\leqslant5\times10^4$), we have observed isolated grooves in a surface profile that seem to be responsible for a generic instability (a rapid growth of the magnitude of the height in a local region of the system) leading to the multiscaling [53].

When the temperature $k_BT/J=1$, however, the distribution is well approximated by Gaussian with $\eta_+=\eta_-=2$, and we have obtained $\zeta=1$, $z=4$, $\kappa\sim0$ with $G(r=1,t)$

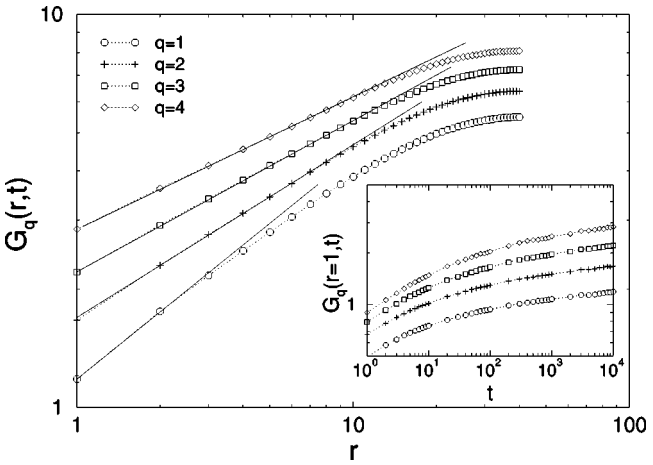

FIG. 10. The qth-order height-height correlation function $G_q(r,t)$ for the (2+1)D MBE model at $t=10^4$. The inset shows the qth-moment step-size function $G_q(r=1,t)$. Here, $L=80$, $k_BT/J=0.234$, and $D/F=10^2$. The solid lines in (a) are power-law fits to the data, yielding $\alpha_q=0.58\pm0.02,0.45\pm0.01,0.38\pm0.01$, and 0.33 ± 0.01 for $q=1-4$, respectively.

$\sim \ln(t)$, and $S \approx 0$. These results are well explained by the MH equation given in Eq. (17) and also agree with the theoretical solution of the distribution for the MH equation that has no up-down symmetry breaking term and yields a Gaussian distribution [3]. Note that for this temperature, we observe no multiscaling behavior from our calculation of $G_q(r,t)$ for $L=80$ at $t=10^4$. It is known that the large curvature (LC) model [24,54] is also well explained by the MH equation (which indicates that the height distribution we consider here is also Gaussian) with a Gaussian step size distribution [24]. The LC model exhibits anomalous scaling with $\kappa \approx 1$ in (1+1)D [$\kappa \approx 0$ with $G(r=1,t) \sim \ln(t)$ in (2+1)D] but no multiscaling [24], which is in good agreement with our result for $k_B T/J=1$. These results provide an important clue for the deviation from $\eta_+ + \eta_- \approx 4$, observed in the models we studied here—that is, the multiscaling is responsible for the deviation regardless of the presence of anomalous scaling.

At this moment, it is unclear to us why $\eta_+ + \eta_- \approx 4$ does not hold (and instead $\eta_+ + \eta_- < 4$) for a model exhibiting multiscaling. We suspect that the deviation from $\eta_+ + \eta_- \approx 4$ for the models we discussed in this section may result from the invalidity of the central limit theorem due to the generic instability, but it does not explain why $\eta_- = 1$ for such models. Furthermore, finding a theoretical height distribution that explains the reason seems to be a very formidable task since one needs to solve a Langevin equation that possibly has an infinite number of marginal operators. However, if the multiscaling is nonuniversal and transient as shown in Refs. [5,25,53] for the DT model, then we expect to recover $\eta_+ + \eta_- \approx 4$ in the long-time asymptotic regime.

IV. SUMMARY AND CONCLUSION

Using extensive simulations of several well-known growth models, we have studied the normalized height distribution that is a fundamental quantity in a study of nonequilibrium surface roughening phenomena. Scaled distributions of the models are obtained, and the shape of each distribution is discussed in terms of the interfacial width, skewness, and kurtosis. We find a simple functional form that explains size-dependent behavior of the skewness and kurtosis in the transient regime, and obtain the transient- and long-time values of the skewness and kurtosis for the models. We show that the strength of the skewness determines the magnitude of the deviation from Gaussian, i.e., asymmetry of the distribution, and that the normalized height distribution can be used to extract the exponents characterizing the universality class of the system. A detailed shape of a distribution has been determined from an exponential fitting, yielding the exponents η_+ and η_-.

Not surprisingly, seemingly different growth models yield the same shape distribution if they belong to the same universality class; the interfacial width, skewness, and kurtosis determine the shape of the distribution. Another important finding is that the sum of the exponents η_+ and η_- is $\eta_+ + \eta_- \approx 4$, and this result is confirmed not only in our simulations of models obeying usual scaling but also in theoretical solutions of continuum growth equations that are available at this moment [3,41]. However, we found a deviation from the sum rule for models exhibiting anomalous scaling as well as multiscaling—that is, $\eta_+ + \eta_- < 4$ with $\eta_- = 1$. Based on the result that the sum is $\eta_+ + \eta_- \approx 4$ for models [e.g., the LC model and the (2+1)D MBE model at the temperature $k_B T/J=1$] exhibiting anomalous scaling but no multiscaling, we believe that the deviation from $\eta_+ + \eta_- \approx 4$ results from the presence of multiscaling in the models that we used here. For the DT and WV models as well as the (2+1)D MBE model at the temperature $k_B T/J=0.234$, the multiscaling (as well as anomalous scaling) is nonuniversal and transient. Thus, in the long-time asymptotic limit, we expect to recover $\eta_+ + \eta_- \approx 4$ for the models.

The height distribution of Ag films grown on a Si substrate is Gaussian with $\zeta = 0.7 \pm 0.1$ [31]. The experimental value of the roughness exponent is in good agreement with our finding in the homoepitaxial thin-film growth model at the temperature $k_B T/J=0.234$, and is close to the theoretical prediction of the Lai-Das Sarma-Villain (LDV) equation that contains an explicit nonlinear symmetry-breaking term. The Gaussian height distribution in the experiment, however, indicates that the asymptotic skewness is zero and there is no multiscaling behavior present in contrast to our result for a small system. Although we do not know the detailed growth mechanisms of the system in the experiment leading to such a similar exponent to the theory, if the LDV equation is a possible growth equation describing the experimental result, then the fourth-order nonlinear term in the equation probably does not play a role in the asymptotic height distribution [like the second-order nonlinear term in the KPZ equation in (1+1)D] and results in the same Gaussian distribution as that for the MH equation, but this needs to be verified by a theory.

It will be interesting to examine the height distribution of growing surfaces in experiment, especially for the cases known to exhibit anomalous scaling. This will provide some more valuable information for our understanding of nonequilibrium surface growth and shed light on the deep connection between the height evolution and its dynamic scaling.

ACKNOWLEDGMENTS

This work was supported by the National Science Foundation under Grant No. DMR-9727714 at the University of Georgia.

[1] *Dynamics of Fractal Surfaces*, edited by F. Family and T. Vicsek (World Scientific, Singapore, 1991).

[2] A.-L, Barabasi and H. E. Stanley, *Fractal Concepts in Surface Growth* (Cambridge University Press, Cambridge, 1995) and references therein.

[3] T. Halpin-Healy and Y. C. Zhang, Phys. Rep. **254**, 215 (1995) and references therein.

[4] J. Krug, *Scale Invariance, Interfaces and Nonequilibrium Dy-*

namics, edited by A. J. McKane, M. Droz, J. Vannimenus, and D. E. Wolf (Plenum, New York, 1995), and references therein.
[5] S. Das Sarma and P. Punyindu, Phys. Rev. E **55**, 5361 (1997).
[6] F. Family and T. Viscek, J. Phys. A **18**, L75 (1985).
[7] S. F. Edwards and D. R. Willkinson, Proc. R. Soc. London, Ser. A **381**, 17 (1982).
[8] M. Kardar, G. Parisi, and Y. C. Zhang, Phys. Rev. Lett. **56**, 889 (1986).
[9] D. E. Wolf and J. Villain, Europhys. Lett. **13**, 389 (1990).
[10] S. Das Sarma and P. Tamborenea, Phys. Rev. Lett. **66**, 325 (1991).
[11] Z. -W. Lai and S. Das Sarma, Phys. Rev. Lett. **66**, 2348 (1991).
[12] M. Eden, in *Proceedings of the Fourth Berkeley Symposium on Mathematical and Statistical Problems*, edited by F. Neyman (University of California Press, Berkeley, 1961).
[13] M. J. Vold, J. Colloid Sci. **14**, 168 (1959).
[14] J. M. Kim and J. M. Kosterlitz, Phys. Rev. Lett. **62**, 2289 (1989).
[15] M. Plischke, J. D. Shore, M. Schroeder, M. Siegert, and D. E. Wolf, Phys. Rev. Lett. **71**, 2509 (1993).
[16] M. Schroeder, M. Siegert, D. E. Wolf, J. D. Shore, and M. Plischke, Europhys. Lett. **24**, 563 (1993).
[17] S. Das Sarma, S. V. Ghaisas, and J. M. Kim, Phys. Rev. E **49**, 122 (1994).
[18] H. -N. Yang, G. -C. Wang, and T. -M. Lu, Phys. Rev. Lett. **73**, 2348 (1994).
[19] J. H. Jeffries, J. -K. Zuo, and M. M. Craig, Phys. Rev. Lett. **76**, 4931 (1996).
[20] J. M. López and J. Schmittbuhl, Phys. Rev. E **57**, 6405 (1998).
[21] A. Brú, J. M. Pastor, I. Fernaud, I. Brú, S. Melle, and C. Berenguer, Phys. Rev. Lett. **81**, 4008 (1998).
[22] S. Morel, J. Schmittbuhl, J. M. López, and G. Valentin, Phys. Rev. E **58**, 6999 (1998).
[23] S. Huo and W. Schwarzacher, Phys. Rev. Lett. **86**, 256 (2001).
[24] J. Krug, Phys. Rev. Lett. **72**, 2907 (1994).
[25] A. Kundagrami, C. Dasgupta, P. Punyindu, and S. Das Sarma, Phys. Rev. E **57**, R3703 (1998).
[26] D. A. Huse, C. L. Henley, and D. S. Fisher, Phys. Rev. Lett. **55**, 2924 (1985).
[27] J. Krug and H. Spohn, Europhys. Lett. **8**, 219 (1989).
[28] G. Parisi, J. Phys. (France) **51**, 1595 (1990).
[29] W. M. Tong, R. S. Williams, A. Yanase, Y. Segawa, and M. S. Anderson, Phys. Rev. Lett. **72**, 3374 (1994).
[30] E. Hahn, H. Schief, V. Marsico, A. Fricke, and K. Kern, Phys. Rev. Lett. **72**, 3378 (1994).
[31] C. Thompson, G. Palasantzas, Y. P. Feng, S. K. Sinha, and J. Krim, Phys. Rev. B **49**, 4902 (1994).
[32] M. C. Bartelt and J. W. Evans, Phys. Rev. Lett. **75**, 4250 (1995).
[33] J. M. Kim, M. A. Moore, and A. J. Bray, Phys. Rev. A **44**, 2345 (1991).
[34] S. Das Sarma, C. J. Lanczycki, R. Kotlyar, and S. V. Ghaisas, Phys. Rev. E **53**, 359 (1996).
[35] For a random variable with zero mean X the first three cumulants are equal to the moments $\langle X^n\rangle_c=\langle X^n\rangle$ for $n\leqslant 3$, and the normalized third and fourth cumulants are $\langle X^3\rangle_c/\langle X^2\rangle_c^{3/2}=\langle X^3\rangle/\langle X^2\rangle^{3/2}$ and $\langle X^4\rangle_c/\langle X^2\rangle_c^2=\langle X^4\rangle/\langle X^2\rangle^2-3$, respectively [from J. Krug, P. Meakin, and T. Halpin-Healy, Phys. Rev. A **45**, 638 (1992)].
[36] M. Kardar, Nucl. Phys. B **290**, 582 (1987).
[37] M. Kotrla and P. Šmilauer, Phys. Rev. B **53**, 13 777 (1996).
[38] Y. Shim and D. P. Landau (to be published).
[39] J. K. Bhattacharjee, S. Das Sarma, and R. Kotlyar, Phys. Rev. E **53**, R1313 (1996).
[40] J. W. Evans and M. C. Bartelt, Langmuir **12**, 217 (1996).
[41] Y. -C. Zhang, Phys. Rev. B **42**, 4897 (1990).
[42] F. Family, J. Phys. A **19**, L441 (1986).
[43] T. Nattermann and L.-H. Tang, Phys. Rev. A **45**, 7156 (1992).
[44] S. Pal and D. P. Landau, Physica A **267**, 406 (1999).
[45] J. Krug, M. Plischke, and M. Siegert, Phys. Rev. Lett. **70**, 3271 (1993); P. Šmilauer and M. Kotrla, Phys. Rev. B **49**, 5769 (1994).
[46] W. W. Mullins, J. Appl. Phys. **28**, 333 (1957); C. Herring, *ibid.* **21**, 301 (1950).
[47] J. Villain, J. Phys. I **1**, 19 (1991).
[48] M. Siegert and M. Plischke, Phys. Rev. E **50**, 917 (1994).
[49] W. H. Press, B. P. Flannery, S. A. Teukolsky, and W. T. Vetterling, *Numerical Recipes* (Cambridge University Press, New York, 1992).
[50] R. Kubo, M. Toda, and N. Hashitsume, *Statistical Physics II* (Springer-Verlag, Heidelberg, Germany, 1985).
[51] We obtained $\kappa_q(\alpha_q)=0.58\pm0.01(0.94\pm0.01), 0.72\pm0.01(0.73\pm0.01), 0.87\pm0.01(0.61\pm0.01)$, and $0.96\pm0.01(0.53\pm0.01)$, respectively, for $q=1-4$, yielding $\kappa_q+\alpha_q\approx 3/2$, where $z=3.8$ was used.
[52] The structure factor is defined as $S_f(\mathbf{k},t)=\langle\hat{h}(\mathbf{k},t)\hat{h}(-\mathbf{k},t)\rangle$ with $\hat{h}(\mathbf{k},t)=(1/L)\Sigma_{\mathbf{r}}[h(\mathbf{r},t)-\langle h\rangle]\exp[-i\mathbf{k}\cdot\mathbf{r}]$ for a two-dimensional substrate. In the asymptotic regime, $S_f(k)\sim L^{\chi}k^{-\gamma}$ with $\chi=0.34$ and $\gamma=3.05$. The nonzero χ indicates the presence of anomalous scaling.
[53] C. Dasgupta, S. Das Sarma, and J. M. Kim, Phys. Rev. E **54**, R4552 (1996); C. Dasgupta, J. M. Kim, M. Dutta, and S. Das Sarma, *ibid.* **55**, 2235 (1997).
[54] J. M. Kim and S. Das Sarma, Phys. Rev. Lett. **72**, 2903 (1994).